NANO MICRO small

Supporting Information

for *Small,* DOI: 10.1002/smll.202205355

Phase Separation–Controlled Assembly of Hierarchically Porous Aramid Nanofiber Films for High-speed Lithium-Metal Batteries

Arum Jung, Michael J. Lee, Seung Woo Lee, Jinhan Cho, Jeong Gon Son, and Bongjun Yeom**

Supporting Information

Phase Separation–controlled Assembly of Hierarchically Porous Aramid Nanofiber Films for High-speed Lithium-metal Batteries

Arum Jung, Michael J. Lee, Seung Woo Lee, Jinhan Cho, Jeong Gon Son, Bongjun Yeom**

Arum Jung, Prof. Bongjun Yeom
Department of Chemical Engineering
Hanyang University
222 Wangsimni-ro, Seongdong-gu, Seoul 04763, Republic of Korea
E-mail: byeom@hanyang.ac.kr

Michael J. Lee, Prof. Seung Woo Lee
George W. Woodruff School of Mechanical Engineering,
Georgia Institute of Technology,
Atlanta, GA 30332, USA

Prof. Jinhan Cho
Department of Chemical and Biological Engineering
Korea University
145 Anam-ro, Seongbuk-gu, Seoul 02841, Republic of Korea

Prof. Jinhan Cho, Dr. Jeong Gon Son
KU-KIST Graduate School of Converging Science and Technology
Korea University
145 Anam-ro, Seongbuk-gu, Seoul 02841, Republic of Korea

Dr. Jeong Gon Son
Soft Hybrid Materials Research Center,
Korea Institute of Science and Technology (KIST)
5 Hwarangno 14-gil, Seongbuk-gu, Seoul 02792, Republic of Korea
Email: jgson@kist.re.kr

*Corresponding author

Prof. Bongjun Yeom

E-mail: byeom@hanyang.ac.kr

Dr. Jeong Gon Son

Email: jgson@kist.re.kr

Table S1. Summary of the recent research in Li metal battery. Previous studies are listed in decreasing order of C-rate.

	Separator	Anode/Cathode	Retention of discharge capacity [%]	C-rate / cycle no.	Ref.
	EPANF	Li/ $LiFePO_4$ (LFP)	83.2 84.5 86.3	10 C / 1000 20 C / 1000 30 C / 1000	This work
1	Reduced graphene oxide coated aramid separator	Li/LFP with N-doped carbon and rGO	79.1	20 C / 1000	Gong *et al*, *Adv. Energy Mater.***2020**,2001479
2	Graphene-coated aramid attached to uncoated aramid	Li/LFP	82.13	20 C / 1000	Gong *et al*, *Energy Environ. Sci.***2021**,*14*,940-954
3	Nanoporous polymer-ceramic composite (PVDF-HFP/Al_2O_3/PVDF-HFP)	Li/LTO	92.3	5 C / 1000	Tu *et al*, *Adv. Energy Mater.***2013**,1300654
4	Polydopamine-treated carbon fiber-coated separator	Li/$LiMn_2O_4$ (LMO)	75.7	2 C / 200	Oh *et al*, *Journal of Power Sources.***2019,***430*,130–136
5	Sulfated zirconia superacid coated PE	Li/ $LiNi_{0.33}Co_{0.33}Mn_{0.33}O_2$ (LNMC)	83	1 C / 150	Woo *et al*, *Energy Environ. Sci.***2021**,*14*,1420
6	Hydroxyapatite coating on PP	Li/ LFP	89	1 C / 500	Yue *et al*, *ACS Appl. Mater. Interfaces*.**2020**,*12*, 43543−43552
7	LiAl LDH-modified PP	Li/LFP	78.6	1 C / 500	Lei *et al*, *Chemical Engineering Journal.***2020**,*395*,125187
9	Aramid Nanofibers coated PP	Li/LMO	85.3	0.5 C / 300	Hu *et al*, *J. Mater. Chem. A*.**2016**,*4*,3513
10	ANF/poly(ethylene oxide) film	Li/ $LiCoO_2$	98	0.25 C / 50	Tung *et al*, *Nature Comm.***2015**,6,6152
11	Cellulose-based porous membrane	Li/S	33.1	0.2 C / 1000	Yu *et al*, *ACS Energy Lett.***2016**,1,633−637
12	Niobium metal particles coated PP	Li/LNMC	78.8	0.2 C / 120	Din. *et al*, *Scientific Reports.***2019**,*9*,16795
13	Aramid nanofibers films	Li/LNMC	68.9	3 mA g^{-1} / 50	Patel *et al*, *ACS Appl. Mater. Interfaces.***2020**,*12*, 25756−25766

Table S2. Porous properties for the PANF samples, and commercial PP.

	Porosity[a] [%]	Pore size[b] [nm]	BET area[c] [m^2 g^{-1}]	Pore volume[b] [cm^3 g^{-1}]
DPANF	54.3±2.0	19.6	2.6	0.013
EPANF	97.2±0.1	11.2	81.6	0.228
IPANF	98.4±0.1	13.1	31.7	0.124
EPANF100	98.3±0.1	13.0	89.7	0.290
EPANF150	96.4±0.1	14.2	97.7	0.356
Commercial PP	47.6±1.0	9.8	21.1	0.054

[a]Obtained using Equation 1. [b]Determined using the Barrett–Joyner–Halenda method.
[bc]Determined using the BET method.

Table S3. Table with the elastic moduli, ultimate strength, and ultimate strain values of the samples. The ultimate strains of the commercial PP samples were out of the d etection range of the testing machine. The mechanical properties of the commercial PP samples in the dry and wet states were not different because of their non-wettability for the liquid electrolytes.

	Ultimate strain [%]	Ultimate strenth [MPa]	Elastic modulus [MPa]
EPANF-dry	3.3±0.8	5.6±0.9	270±20
EPANF-wet	9.5±0.8	3.3±0.8	170±50
EPANF100-dry	4.6±1.0	6.7±0.6	300±60
EPANF100-wet	7.7±2.1	3.6±0.4	150±40
EPANF150-dry	6.2±1.0	6.5±0.6	230±20
EPANF150-wet	9.8±1.1	1.4±0.1	770±70
Commercial PP-MD	-	87±6	770±70
Commercial PP-TD	-	7.5±0.2	290±20

Table S4. Bulk resistances and ionic conductivities obtained from Fig. 3i.

	Thickness[a] [μm]	R_b [Ohm]	σ [mS cm^{-1}]	E_a [kJ mol^{-1}]
EPANF	20	0.42	1.87	12.3
EPANF100	40	0.66	2.38	14.1
EPANF150	70	0.68	4.04	16.5
Commercial PP	25	0.84	1.17	14.0

[a]Obtained from FE-SEM.

Table S5. Chemical compositions of the samples in Fig. 6.

Name	EPANF before immersion [Atomic %]	EPANF after immersion [Atomic %]	Commercial PP before immersion [Atomic %]	Commercial PP after immersion [Atomic %]
Li1s	0	0	0	1.2
P2p	0	0.6	0	0
C1s	78.0	74.9	94.6	97.3
N1s	11.1	10.3	0	0
O1s	10.9	11.6	5.4	1.1
F1s	0	2.6	0	0.4

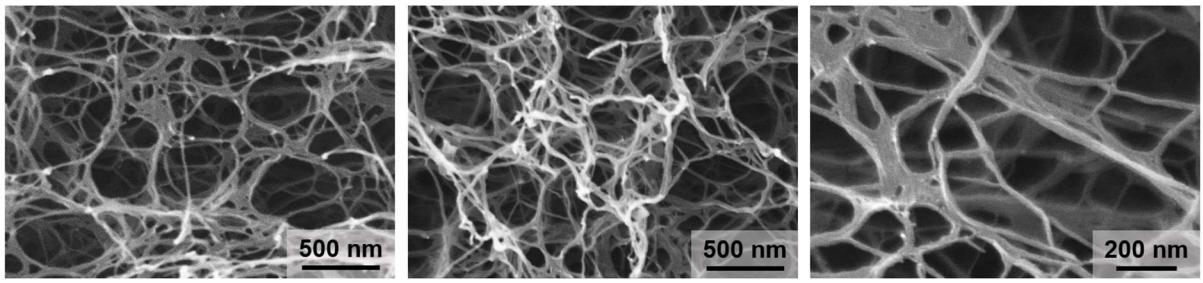

Figure S1. High-magnification FE-SEM images of EPANF cross-sections at different locations.

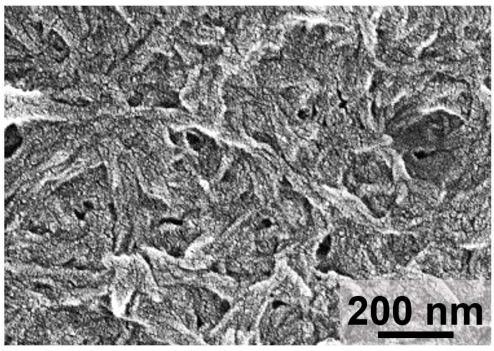

Figure S2. Magnified FE-SEM image of the EPANF sample.

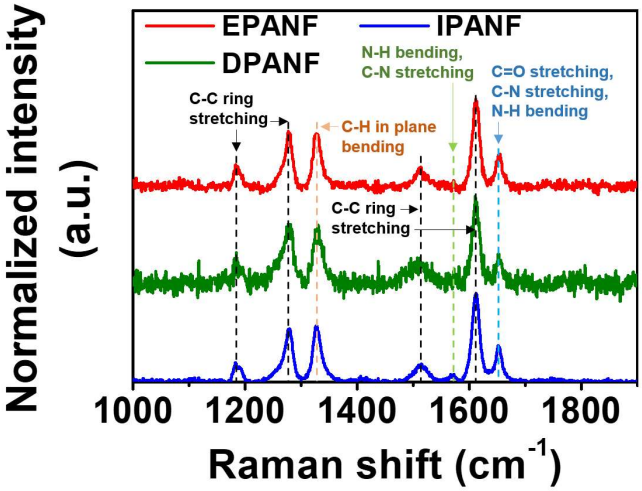

Figure S3. Raman spectra of EPANF, DPANF, and IPANF.

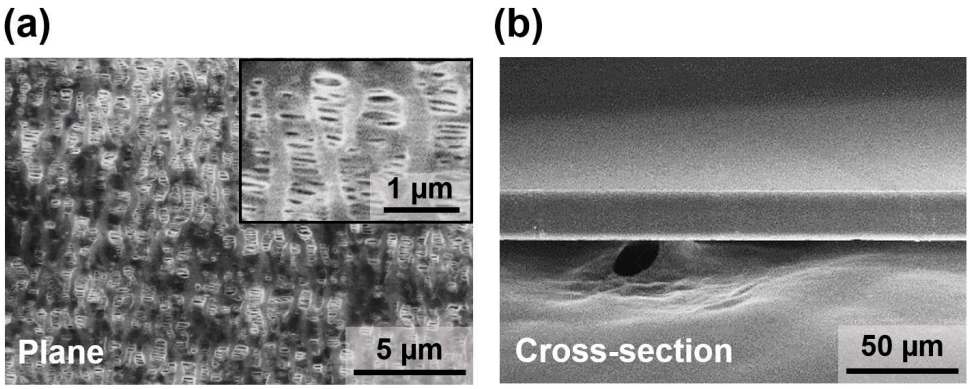

Figure S4. FE-SEM images of commercial PP. Plane surface images are shown in a), and higher magnification images are placed in the insets. Cross-sectional images are shown in b).

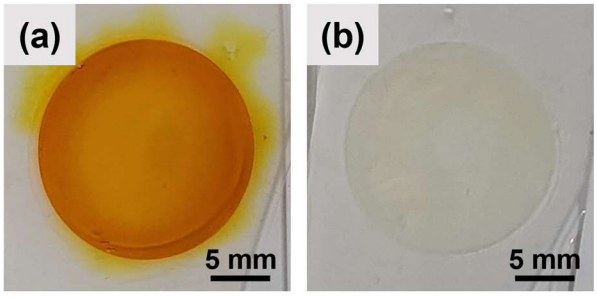

Figure S5. Photographs of (a) casted aramid sol film and (b) gel-state aramid film after immersion in DI water.

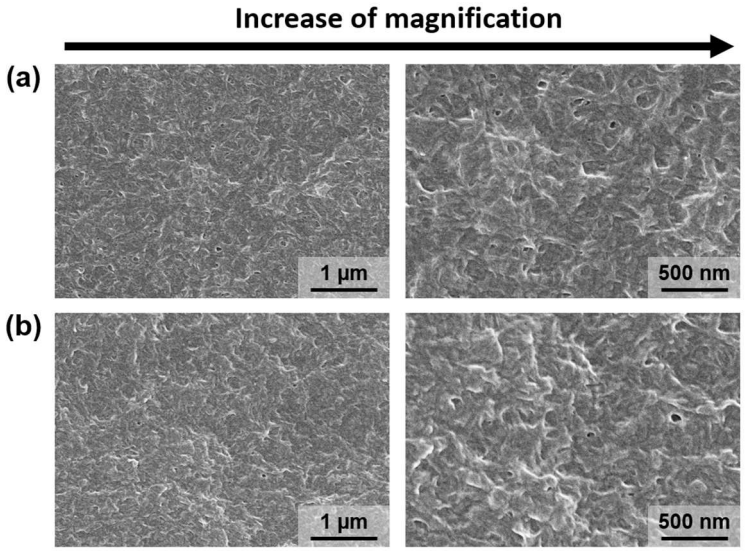

Figure S6. FE-SEM images of a) aramid film prepared by single-exchange process with DI water and b) DPANF. The thicknesses of the films in a) and b) were similar to 6.4±0.5 μm and 6.6±0.8 μm, respectively.

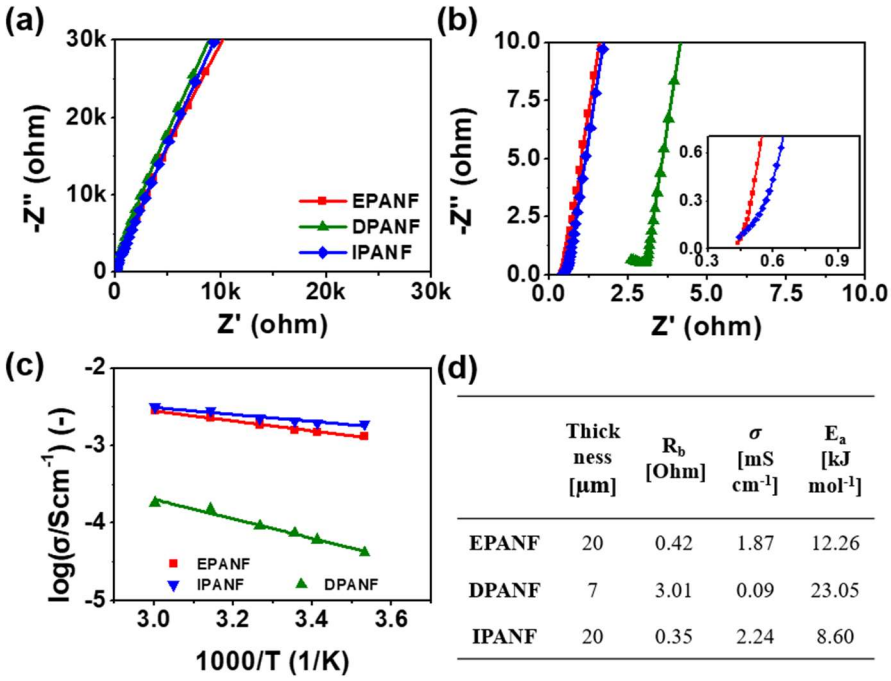

	Thickness [μm]	R_b [Ohm]	σ [mS cm^{-1}]	E_a [kJ mol^{-1}]
EPANF	20	0.42	1.87	12.26
DPANF	7	3.01	0.09	23.05
IPANF	20	0.35	2.24	8.60

Figure S7. a) EIS results for SS/SS cells with EPANF (red squares), DPANF (green triangles), and IPANF (blue rhombuses) at 33 °C. b) Magnification of plots in a) near origin. c) Arrhenius plots for conductivity as function of temperature. Each line represents the results fitted using Equation 3. d) Table showing bulk resistances, ionic conductivities, and activation energies of separators obtained from a) and b). Thicknesses were obtained from FE-SEM images.

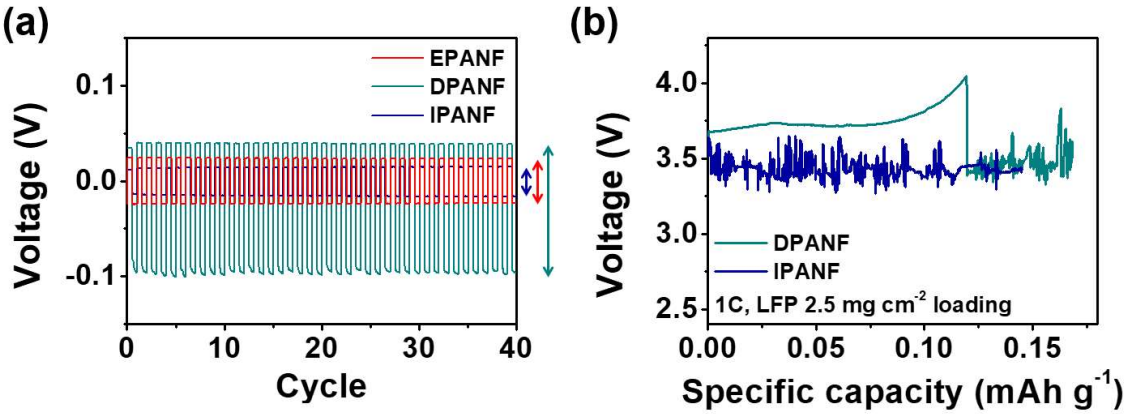

Figure S8. a) Symmetric cell tests with cycle-voltage profiles at 10 mA cm^{-2} (1 mAh cm^{-2}) for the EPANF, DPANF, and IPANF samples. The profiles for 40 cycles are shown. b) Charge/discharge curves of the LFP/Li cells with DPANF (green line) and IPANF (blue line) at 1 C.

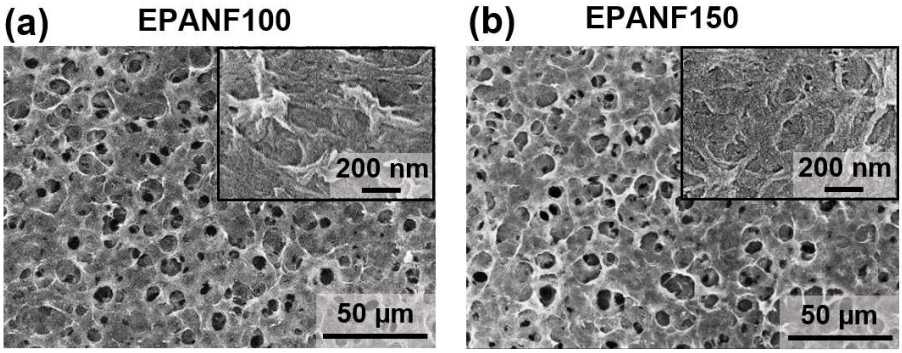

Figure S9. Plane surface images of FE-SEM images of a) EPANF100, and b) EPANF150. Higher magnification images are placed in the insets of each images.

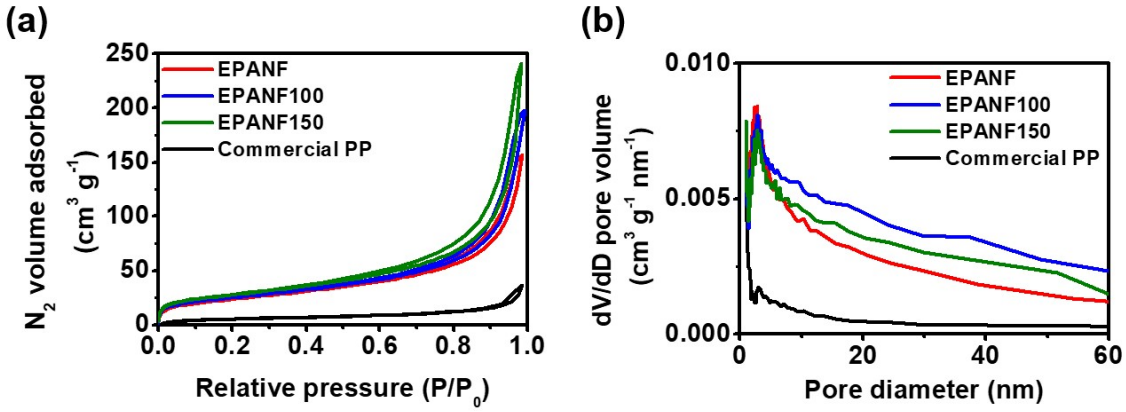

Figure S10. a) BET nitrogen adsorption–desorption isotherms and(b) pore distribution data for EPANF, EPANF100, EPANF150, and commercial PP films.

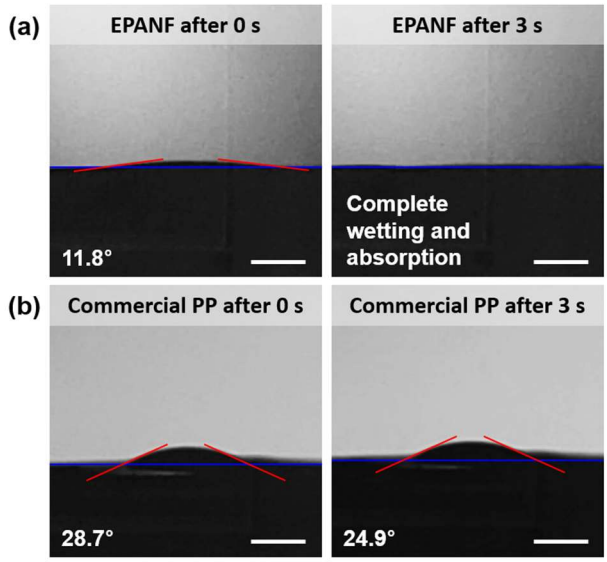

Figure S11. Contact angle tests of the EPANF and commercial PP samples with liquid electrolyte droplets. Scale bar = 2 mm.

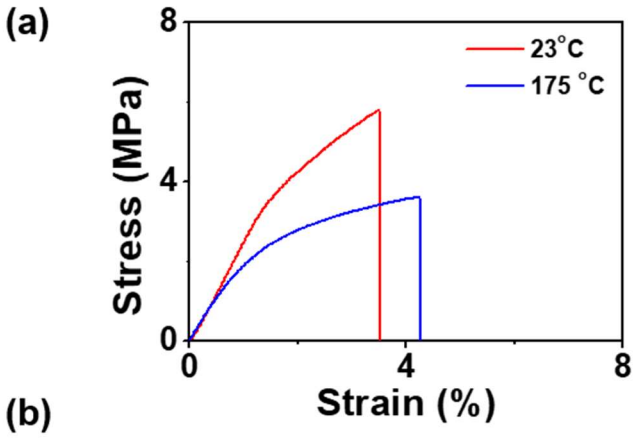

	Elastic modulus [MPa]	Ultimate strength [MPa]	Ultimate strain [%]
23 °C	270±20	5.6±0.9	3.3±0.8
175 °C	210±20	3.6±0.2	3.6±0.7

Figure S12. Results of uniaxial tensile tests for EPANF samples at 23℃ and 175 ℃.

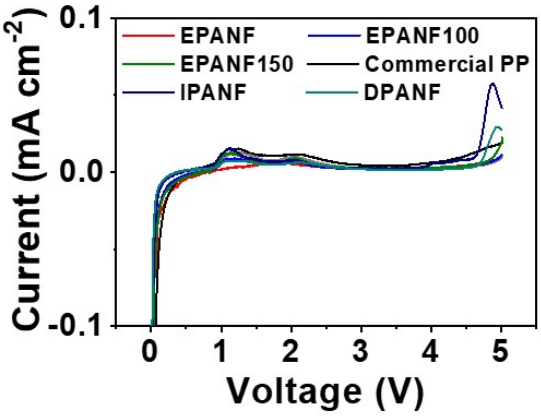

Figure S13. Linear sweep voltammetry of EPANF (red line), EPANF100 (blue line) and EPANF150 (green line), IPANF (navy line), DPANF (dark cyan line), and Commercial PP (black line).

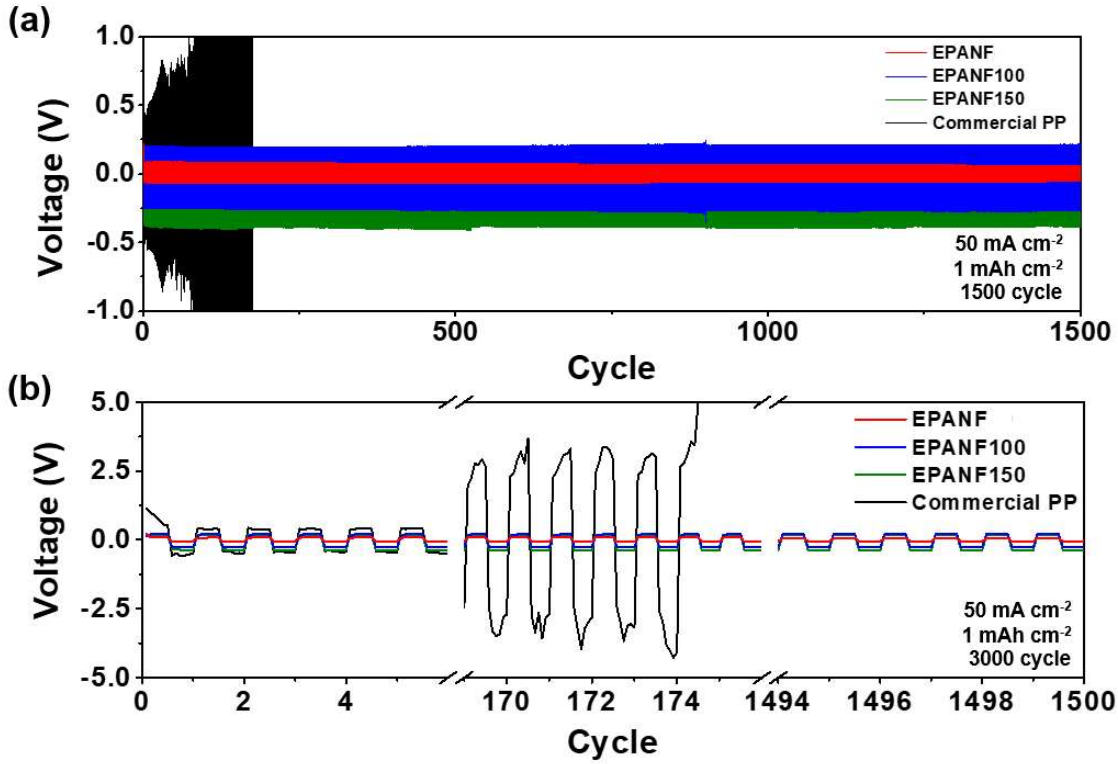

Figure S14. a) Symmetric cell test cycle–voltage profiles for 1500 cycles at 50 mA cm^{-2} (1 mAh cm^{-2}). Selected regions of 0–5, 170–175, and 1495–1500 cycles are shown in b).

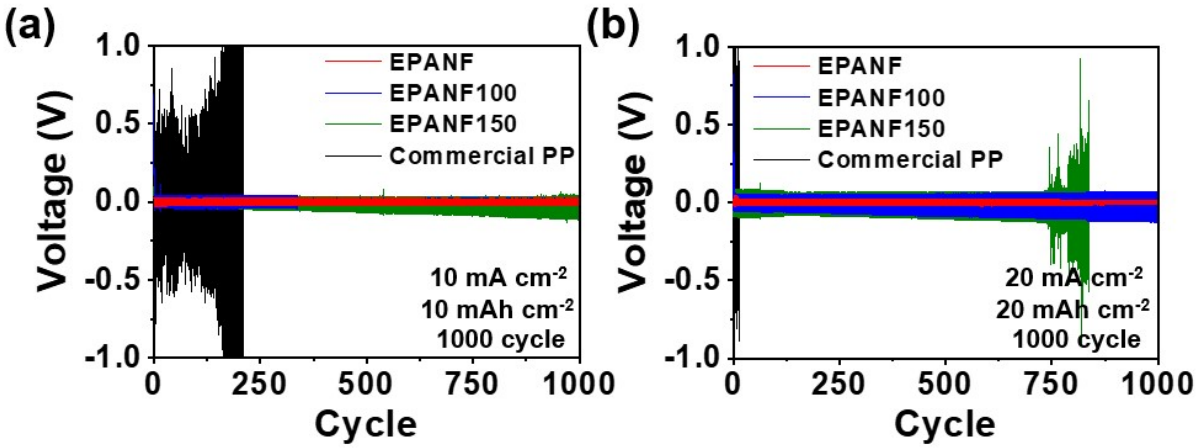

Figure S15. Symmetric tests with higher capacities of a) 10 mA cm^{-2} (10 mAh cm^{-2}), and b) 20 mA cm^{-2} (20 mAh cm^{-2}) for 1000 cycles.

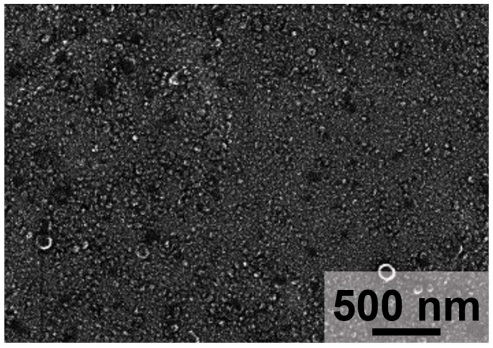

Figure S16. High-magnification FE-SEM image of the Li electrode with EPANF.

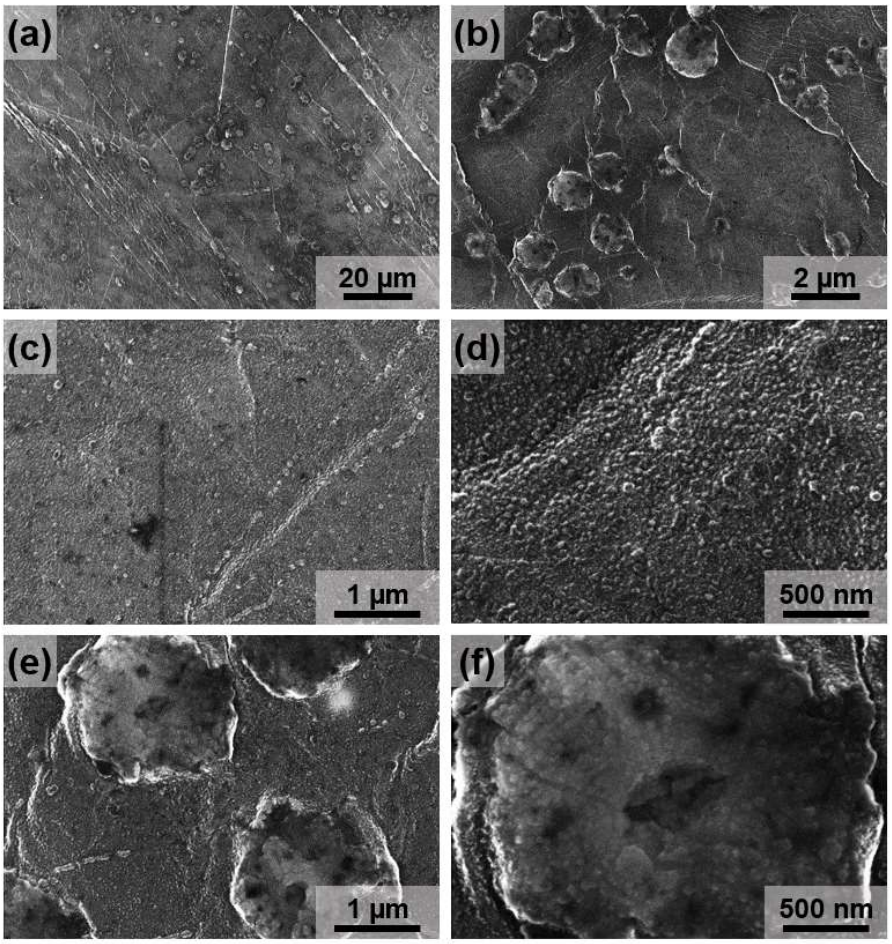

Figure S17. FE-SEM images of the surface of the Li electrode with EPANF after 1000 cycles at 10 mA cm^{-2} (10 mAh cm^{-2}). a–f) The images were obtained at different magnifications.

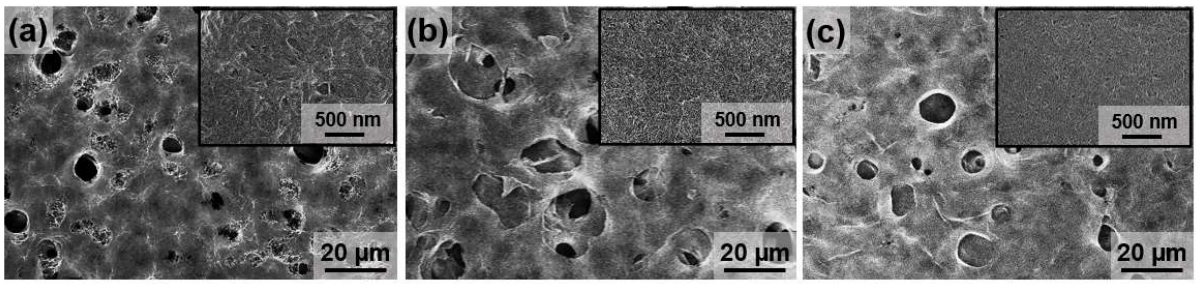

Figure S18. FE-SEM images of the separator surfaces after 100 cycles at 10 mA cm^{-2} (1 mAh cm^{-2}) a) EPANF, b) EPANF100, and c) EPANF150. The insets show the high-magnification images.

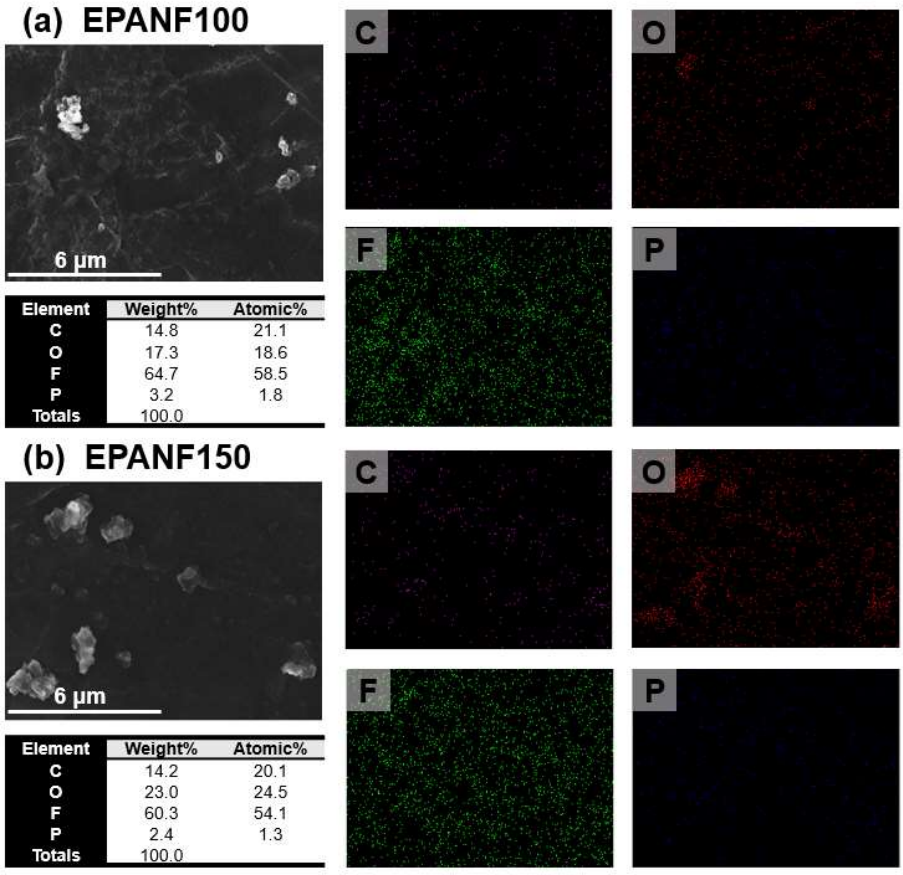

Element	Weight%	Atomic%
C	14.8	21.1
O	17.3	18.6
F	64.7	58.5
P	3.2	1.8
Totals	100.0	

Element	Weight%	Atomic%
C	14.2	20.1
O	23.0	24.5
F	60.3	54.1
P	2.4	1.3
Totals	100.0	

Figure S19. FE-SEM images, EDX results, and elemental mapping images of the Li metal electrode surfaces with a) EPANF100 and b) EPANF150 after 100 cycles at 10 mA cm^{-2} (1 mAh cm^{-2}). The scale bar in the FE-SEM images is 6 μm in length.

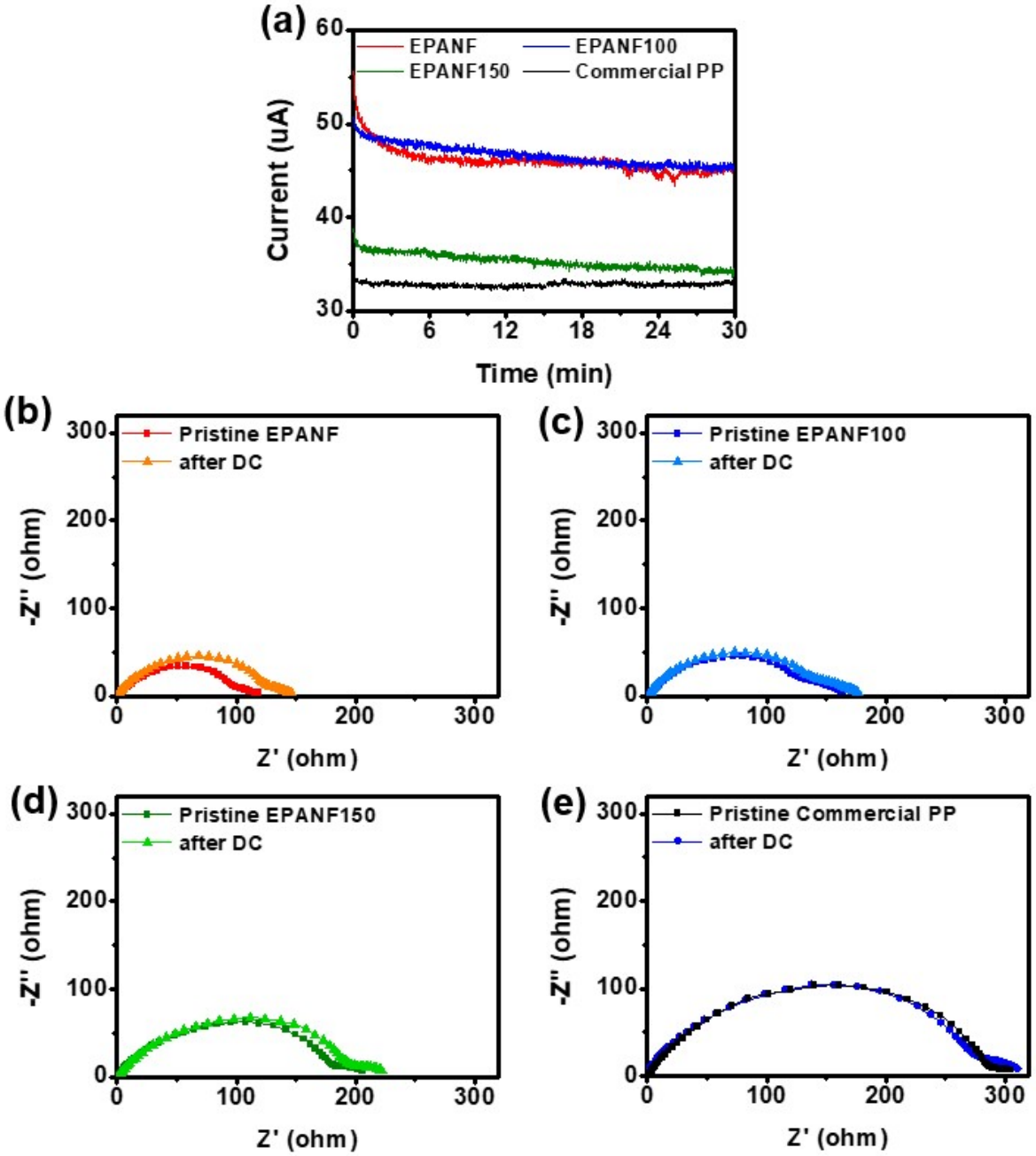

Figure S20. Measurement of the lithium ion transference number. a) DC polarization curves of the Li/Li cells with EPANF (red line), EPANF100 (blue line), EPANF150 (green line), and commercial PP (black line) films. EIS data of b) EPANF, c) EPANF100, d) EPANF150, and e) commercial PP before and after the application of the DC.

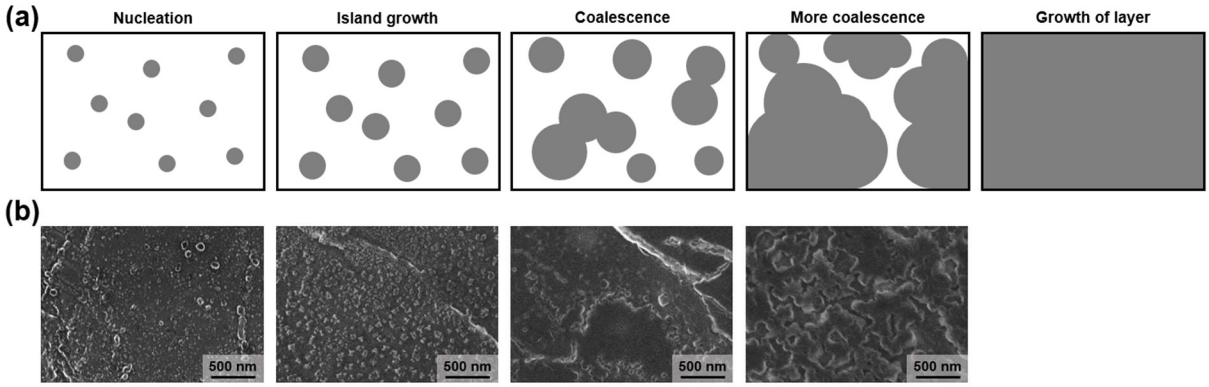

Figure S21. (a) Schematics of Li depositions and growth in layers. (b) FE-SEM images of Li surfaces after 100 cycling tests at 10 mA cm^{-2} with EPANF separators.

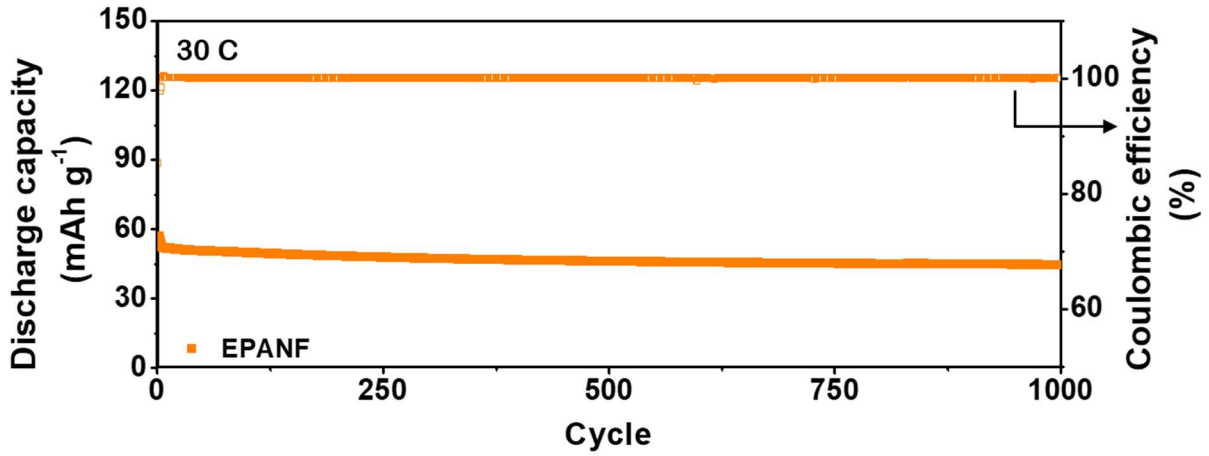

Figure S22. Cycle performances and Coulombic efficiencies of the LFP/Li cells operated at 30 C.

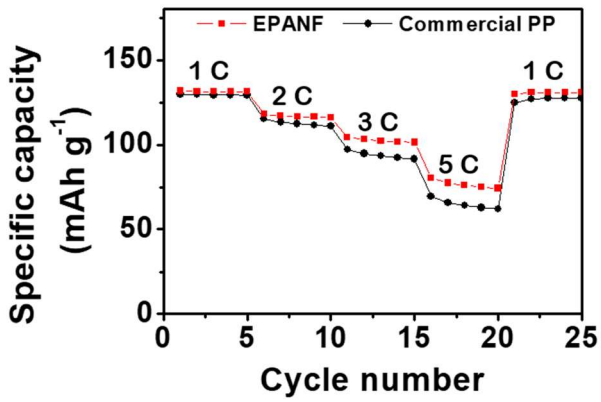

Figure S23. Step cycling tests for LFP/Li cells with the LFP loading mass of 9 mg cm^{-2} at 1 to 5 C rates for EPANF (red color) and commercial PP (black color).